Cell Reports
Medicine

Report

PPRX-1701, a nanoparticle formulation of 6′-bromoindirubin acetoxime, improves delivery and shows efficacy in preclinical GBM models

Graphical abstract

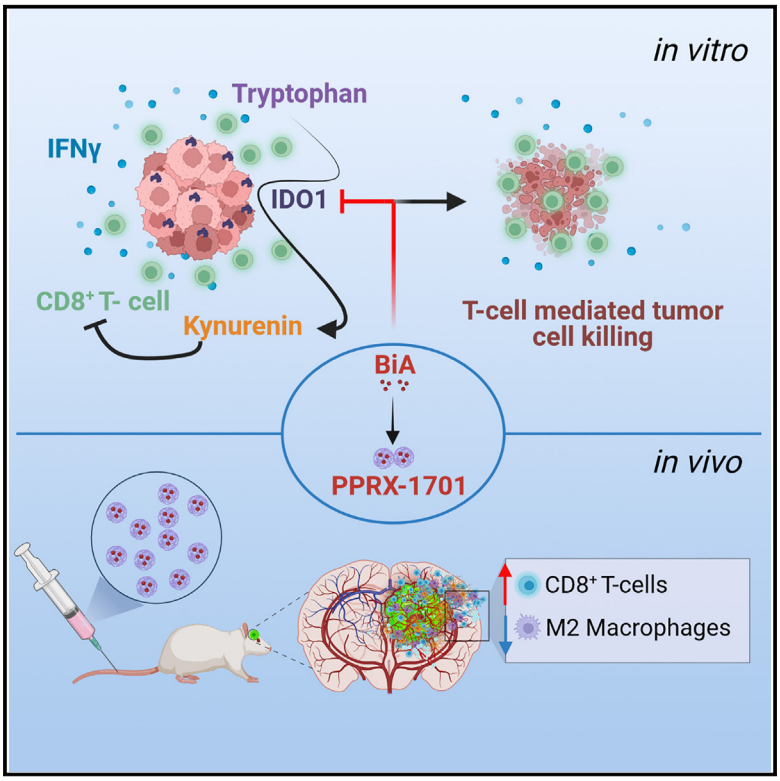

Highlights

- PPRX-1701 is a deliverable formulation of 6-bromoindirubin-3′-acetoxime (BiA)
- Inhibits IDO1 expression and increases CD8 T cell infiltration in GBM mouse models
- Data support investigation of this approach for future potential translation

Authors

Mykola Zdioruk, Jorge-Luis Jimenez-Macias, Michal Oskar Nowicki, ..., Alexander L. Ling, E. Antonio Chiocca, Sean E. Lawler

Correspondence

sean_lawler@brown.edu

In brief

Zdioruk et al. investigate the potential of 6′-bromoindirubin acetoxime (BiA) in treating glioblastoma (GBM) in preclinical mouse models. BiA inhibits immunosuppressive pathways in GBM, while PPRX-1701, a nanoparticle formulation of BiA, improves survival in immunocompetent GBM models. The study suggests that this approach may have potential for future translation in GBM treatment.

Zdioruk et al., 2023, Cell Reports Medicine *4*, 101019
May 16, 2023
https://doi.org/10.1016/j.xcrm.2023.101019

CellPress

Cell Reports Medicine

CellPress
OPEN ACCESS

Report

PPRX-1701, a nanoparticle formulation of 6′-bromoindirubin acetoxime, improves delivery and shows efficacy in preclinical GBM models

Mykola Zdioruk,[1] Jorge-Luis Jimenez-Macias,[1,2] Michal Oskar Nowicki,[1] Katherine E. Manz,[4] Kurt D. Pennell,[4] Marilin S. Koch,[1] Tomer Finkelberg,[1] Bin Wu,[3,5] Paul Boucher,[3] Yuji Takeda,[3] Weiyi Li,[3] Raziye Piranlioglu,[1] Alexander L. Ling,[1] E. Antonio Chiocca,[1] and Sean E. Lawler[1,2,6,*]

[1]Harvey Cushing Neurooncology Laboratories, Department of Neurosurgery, Brigham & Women's Hospital, Harvard Medical School, Boston, MA 02115, USA

[2]Department of Pathology and Laboratory Medicine, Department of Neurosurgery, Legorreta Cancer Center, Brown University, Providence, RI 02903, USA

[3]Phosphorex, Inc, Hopkinton, MA 01748, USA

[4]School of Engineering, Brown University, Providence, RI 02912, USA

[5]Cytodigm, Inc., Hopkinton, MA 01748, USA

[6]Lead contact

*Correspondence: sean_lawler@brown.edu

https://doi.org/10.1016/j.xcrm.2023.101019

SUMMARY

Derivatives of the Chinese traditional medicine indirubin have shown potential for the treatment of cancer through a range of mechanisms. This study investigates the impact of 6′-bromoindirubin-3′-acetoxime (BiA) on immunosuppressive mechanisms in glioblastoma (GBM) and evaluates the efficacy of a BiA nanoparticle formulation, PPRX-1701, in immunocompetent mouse GBM models. Transcriptomic studies reveal that BiA downregulates immune-related genes, including indoleamine 2,3-dioxygenase 1 (IDO1), a critical enzyme in the tryptophan-kynurenine-aryl hydrocarbon receptor (Trp-Kyn-AhR) immunosuppressive pathway in tumor cells. BiA blocks interferon-γ (IFNγ)-induced IDO1 protein expression *in vitro* and enhances T cell-mediated tumor cell killing in GBM stem-like cell co-culture models. PPRX-1701 reaches intracranial murine GBM and significantly improves survival in immunocompetent GBM models *in vivo*. Our results indicate that BiA improves survival in murine GBM models via effects on important immunotherapeutic targets in GBM and that it can be delivered efficiently via PPRX-1701, a nanoparticle injectable formulation of BiA.

INTRODUCTION

Glioblastoma (GBM) is a malignant brain tumor that remains among the most formidable cancers.[1–3] Despite a well-established standard of care of maximal surgical resection followed by radiotherapy plus concomitant temozolomide (TMZ), median survival remains approximately 15 months.[2,4,5] GBM is characterized by the hallmarks of rapid growth, invasion, angiogenesis, heterogeneity, and immunosuppression. In recent years, immunotherapy has emerged as a potentially curative approach for the treatment of some cancers.[6–9] However, clinical trials thus far using these approaches have demonstrated limited efficacy in GBM.[10,11] This may be explained in part by the nature of the GBM tumor microenvironment (TME)—a hypoxic, acidic, and immunosuppressive immune/inflammatory cell-enriched milieu that promotes tumor development and therapy resistance.[12–14]

The GBM TME is characterized by a network of molecular and cellular interactions that support immune evasion.[15] Key molecules involved comprise immunosuppressive cytokines, immune checkpoint molecules including PD-L1, and the metabolic enzyme indoleamine 2,3-dioxygenase 1 (IDO1). At the cellular level, a distinctive TME dominated by myeloid cells and microglia is now emerging as a key GBM hallmark.[16,17] Targeting these elements appropriately could allow the GBM TME to convert from an immunotherapy resistant "cold" to a permissive "hot" cellular ecosystem.[10,18]

We previously identified 6′-bromoindirubin-3′-acetoxime (BiA) as an anti-invasive and anti-angiogenic compound that had therapeutic benefit in human GBM xenograft models in nude mice.[19] BiA is a chemical derivative of indirubin, a natural product present in indigo plants and a constituent of the traditional Chinese medicine Dang Gui Long Hui Wan, which has been used in the treatment of chronic myelogenous leukemia (CML). *In vitro* and animal studies of indirubin and its derivatives have indicated anti-inflammatory, anti-tumor, and neuroprotective effects.[19–21] Mechanistically, BiA and other indirubin analogs act as ATP-competitive protein kinase inhibitors with broad selectivity. Reported high-affinity targets include GSK-3, Src-family, JAK2, and some receptor tyrosine kinases.[19,20,22–25] The clinical development of these compounds has been hampered by poor solubility, which limits bioavailability, efficacy, and delivery.

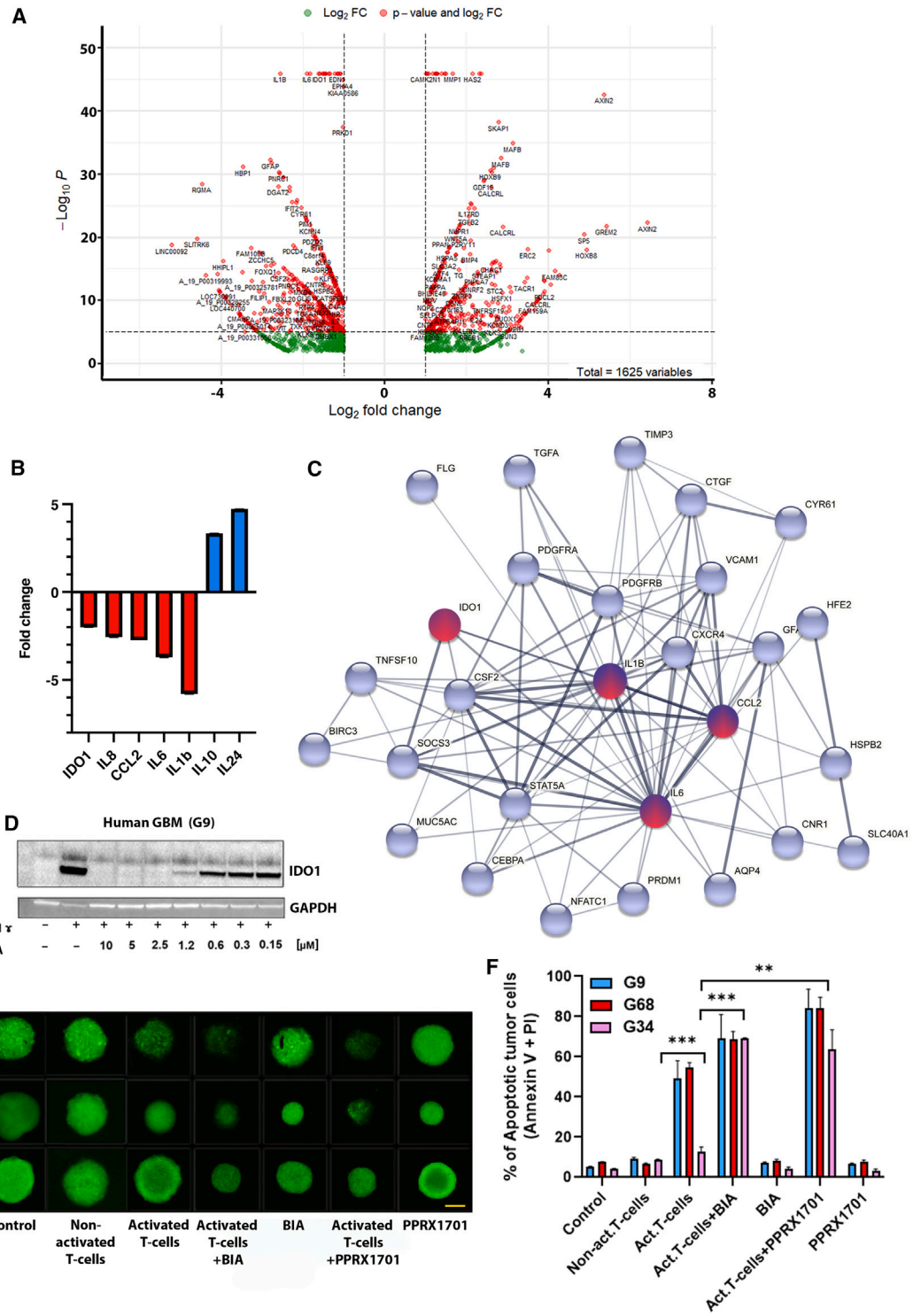

Figure 1. BiA inhibits expression of immunosuppressive genes and sensitizes GBM cells to T cell-mediated killing

(A) Gene expression analysis of U251 cells treated with 1 μM BIO for 24 h and compared with untreated cells. Volcano plot represents a total of 1,625 genes differentially expressed more than 2-fold (log2) after BIO treatment ($p < 0.005$) (n = 3).

(B) Bar graph illustrates expression changes in key dysregulated immunoregulatory genes.

(C) Interaction network map built using STRING v.11.0 and based on the 28 immune related genes clustered out of 500 most downregulated genes after BIO treatment detected in U251 cells. Genes are shown as a nodes, and the existence of interactions between them are represented by edges. Edge thickness indicates the strength of the different interactions. Highlighted nodes represent specific interactions between downregulated genes shown in (B) ($p < 0.0001$).

(legend continued on next page)

PPRX-1701 is a synthetic nanoparticle formulation consisting of submicron particles of BiA within a network of biodegradable poly(lactide-co-glycolide) (PLGA), which allows intravenous delivery. Here, we show that BiA inhibits the expression of IDO1—a key enzyme in the immunosuppressive pathway in GBM TME. Using PPRX-1701, we were able to deliver BiA *in vivo* and block tumor growth in murine GBM models. This was associated with alterations in the TME that suggest potential for anti-tumor immune responses. This study demonstrates the immunomodulatory effects of BiA in GBM, supporting further development of this approach.

RESULTS

BiA blocks expression of IDO1 in GBM cells and improves T cell killing

BiA has shown promising activity in mouse models of GBM; however, the effects of BiA on gene expression in GBM cells have not been examined. Transcriptomic analysis of the effects of the closely related 6-bromo-3′-indirubin oxime (BIO) on GBM cells revealed extensive alterations with 1,625 significantly differentially expressed genes in treated GBM cells compared with untreated controls (Figure 1A; Table S1). STRING pathway analysis of the top 500 downregulated genes (p adjusted < 0.005) showed an interaction network and included a cluster of 28 downregulated genes centered around immunoregulatory functions (Figures 1B and 1C). Several interferon-γ (IFNγ)-regulated genes were identified including IDO1,[26] which is under evaluation preclinically and clinically as an immunotherapeutic target for the treatment of GBM and other cancers. We therefore investigated the effects of BiA on IDO1 induction by IFNγ in GBM cell lines. IFNγ strongly induced IDO1 protein expression which was blocked by BiA treatment in a dose-dependent manner with almost complete suppression at a concentration of 1 μM (Figure 1D). We then investigated the killing of GBM cells mediated by T cells in a co-culture assay.[27] This showed that BiA treatment significantly enhanced T cell-mediated tumor cell killing across three distinct GSC lines and decreased GBM sphere size as a consequence of significantly increased T cell-mediated apoptotic death of tumor cells compared with the control and compared with the activated T cells alone ($p < 0.005$) (Figures 1E and 1F).These results suggest that BiA may sensitize GBM cells to T cell killing by the downregulation of immunosuppressive genes including IDO1.

Characterization of PPRX-1701, a deliverable nanoparticle formulation for systemic administration of BiA

We previously showed that BiA blocks GBM invasion and promotes survival in murine GBM xenografts.[19] However, poor drug solubility in physiological buffers hampered further development of this approach. To overcome this limitation, a formulation for effective *in vivo* intravenous delivery has been developed composed of indirubin and its derivatives in nanoparticles in the size range of tens to hundreds of nanometers (Figure 2A; Figure S1). Such nanosized BiA particles have much larger surface areas, and as a result, their solubility and bioavailability are expected to be greatly improved.

To test the functionality of BiA delivered by PPRX-1701, we performed several *in vitro* tests, including cell viability and cell cycle analysis (Figure S1) as well as GBM proliferation and migration assays (Figures 2B and 2C) where cells were grown in ultra-low-attachment conditions, forming neurospheres or spheres embedded in collagen, and treated with BiA or PPRX-1701 over a range of concentrations. These assays showed significant reduction of proliferation and migration rates in a dose-dependent manner consistent with our previous data.[13] In the context of these assays where delivery and solubility are not limiting factors, PPRX-1701 and BiA were indistinguishable, indicating that they are equivalent in terms of their biological effects. Additionally, to understand the impact of IDO1 inhibition on proliferation and migration of GBM cells we used small interfering RNA (siRNA) to knock down IDO1, which showed that IDO1 silencing has a moderate inhibitory effect on GBM cell motility and proliferation (Figures 2D–2F). Together, these data suggest that BiA inhibition of IDO1 may partially impair cell proliferation and tumor development. However, there are also likely to be more pronounced functions in the TME where IDO1 is induced by IFNγ.

Importantly, the improved solubility of PPRX-1701 compared with BiA allowed us to perform efficacy studies and increase the experimental *in vivo* dosage more than 10 times compared with our previous studies in murine GBM xenografts, where BiA solubility was a limiting factor.[19] First, to determine whether PPRX-1701 can modulate tumor cell biology *in vivo*, we used G9 GBM cells stably transduced with the TOPFlash reporter plasmid.[28] This allows the sensitive detection of bioluminescent signal when cells are treated with BiA via its known inhibition of GSK-3,[29] which leads to β-catenin stabilization, nuclear translocation, and transcription via a TCF/LEF promoter. One hour after delivery of 10 mg/kg PPRX-1701 via tail-vein injection, we were able to detect a luminescent signal in intracranial G9 TOPFlash tumors, indicating *in vivo* delivery of BiA to intracranial tumors (Figure 2G). To further validate these data, we performed mass spectrometry analysis of the tumor tissue with concurrent pharmacokinetic assessment of PPRX-1701 tissue/plasma ratios at different time points after treatment. Our data show that PPRX-1701 can reach intracranial GBM in mice at levels consistent with GSK-3 inhibition and remains readily detectable in tumor tissue up to 5 h after injection, as shown in Figure 2H. Together, the pharmacokinetic and brain/tumor uptake data show *in vivo* delivery of BiA at biologically relevant concentrations via intravenous administration.

(D) Effect of BiA on IDO1 expression in G9 cells induced by IFNγ. Cells were stimulated with 100 ng/mL IFNγ for 24 h ± BiA at different concentrations.
(E and F) BiA enhances T cell-mediated tumor cell killing. Images on day 6 (E) show reduced sphere size and fluorescence intensity for the combination of BiA and activated $CD8^+$ T cells (4× magnification, scale bar: 500 μm). Bar graph shows the apoptotic response from all GSCs for each condition at day 6 of treatment assessed via annexin V and PI staining.
Data are represented as mean ± SD of three replicates.

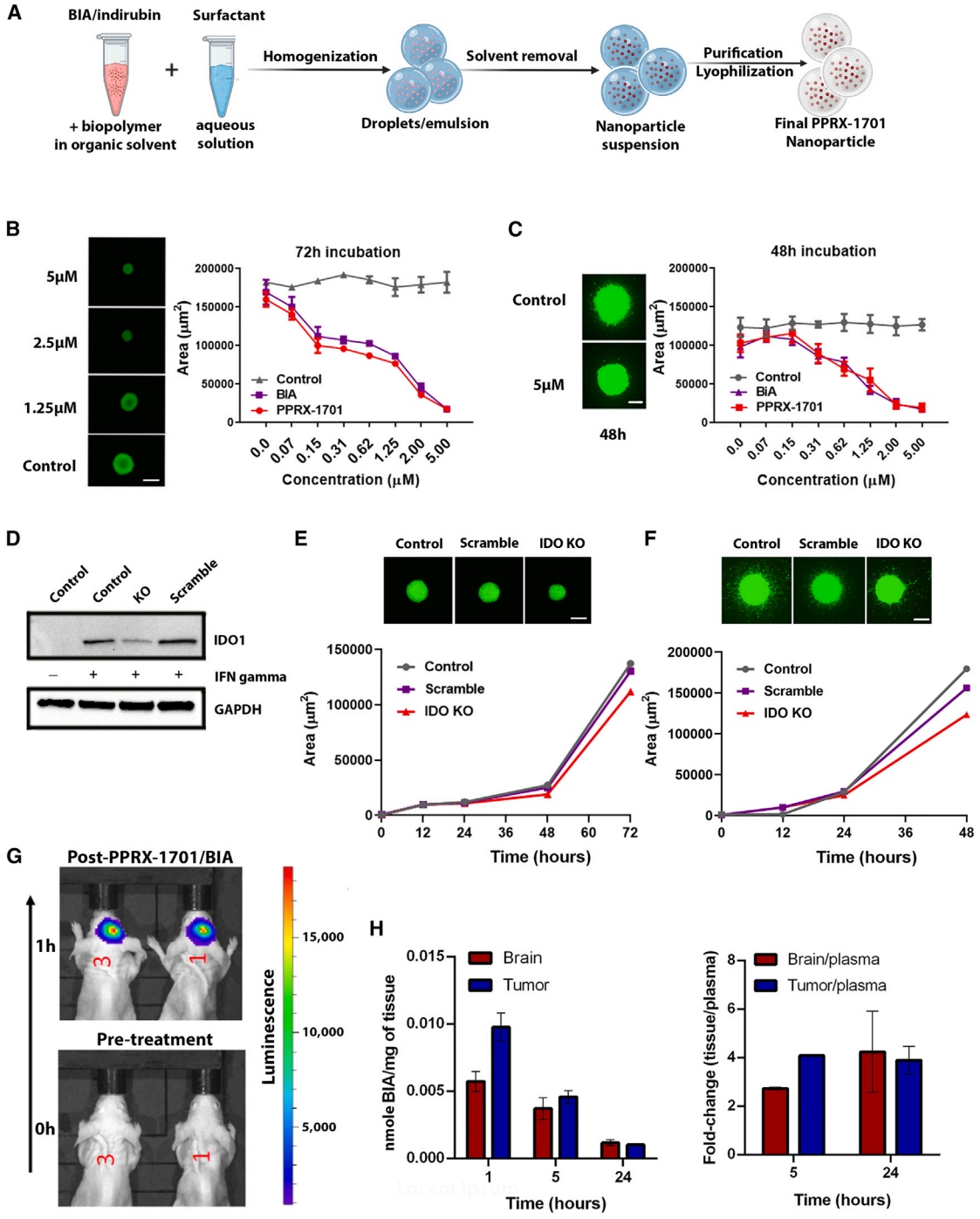

Figure 2. Assessment of effects of PPRX-1701 on GBM cell growth, invasion, and tumor targeting *in vivo*

(A) Diagram illustrating the formulation of PPRX-1701.

(B and C) BiA and PPRX-1701 suppress proliferation and migration of GBM stem cells to a similar extent *in vitro*. The G9 cells were grown for 72 h ± BiA/PPRX-1701. BiA or PPRX-1701 suppressed GSC growth in a dose-dependent manner. This effect correlates with the ability of the BiA to inhibit migration of GBM shown in (C), where GSC spheres were embedded in collagen and treated with BiA or PPRX-1701. Migration rate was measured via sphere size and number of migrated cells. Scale bar: 500 μm.

(D) Western blot shows the level of siRNA silencing (knockout [KO]) of IDO1 G9 GBM cells.

(E and F) IDO1 siRNA has a negative effect on proliferation and migration of GBM cells *in vitro* (scale bar: 500 μm).

(legend continued on next page)

PPRX-1701 blocks IFNγ-mediated upregulation of IDO1 in murine GBM cells and prolongs survival

To determine whether PPRX-1701 may affect tumor progression *in vivo*, we first performed an *in vitro* study to validate inhibitory properties of the PPRX-1701 formulation on IFNγ induction of IDO1 expression in murine GBM cells. Consistent with human GBM cells shown in Figure 1, PPRX-1701 blocked IFNγ-induced expression of IDO1 in both GL261 and CT2A murine GBM cell lines and was several-fold more effective in GL261 cells, as shown in Figure 3A.

To examine the effects of PPRX-1701 on GBM tumor growth, we performed a preclinical *in vivo* study in immunocompetent models using both GL261 and CT2A models according to the plan outlined in Figure 3B. In this preclinical trial, GL261 reflects the role of highly immunogenic "hot" GBM tumor, and CT2A, for comparison, is an immunologically "cold" tumor model. The results of these studies revealed that the GL261 control cohort, injected with vehicle (non-loaded nanoparticles), had a median survival time of 30 days, typical for this model, while animals that received therapy 3 times a week (6 doses of PPRX-1701 in total) at 20 mg/kg survived longer (42 days) (Figure 3C). This represented a significant prolongation of survival compared with the control cohort (log rank test: ***$p = 0.0006$). This observation was also confirmed by magnetic resonance imaging (MRI) (Figure 3D) and by tumor volumetric analysis performed on day 28 after tumor implantation where the tumor volume of the treated animals was 50 mm^3 compared with the control group with an average tumor volume of 100 mm^3 ($p < 0.0001$, $n = 5$) (Figure 3E). These experiments were performed in young mice and reports suggested a higher level of immunosuppression and IDO1 expression in aging adults,[26,30] which is relevant because 90% of GBM cases are diagnosed in patients older than 65 years.[2] Further *in vivo* experiments performed in aged, 7-month-old mice showed that BiA remains effective in this context (Figure S2).

In the CT2A mouse GBM model, treatment with PPRX-1701 led to a small but significant difference in survival (Figure 3F). This model is considered immunologically "cold" and suggests that PPRX-1701 may synergize with therapies that may activate the TME. Also, as shown in Figure 3A, suppression of IDO1 was stronger in GL261 cells than CT2A, suggesting the potential role of this pathway in sensitivity to PPRX-1701.

To determine whether prolonged survival in the GL261 model correlated with intratumoral levels of IDO1, we performed histopathological immunofluorescence analysis of the brain tumor sections. As indicated in Figure 3I, tumor tissue from BiA-PPRX-1701-treated animals showed significantly fewer $IDO1^+$ cells compared with controls. To further confirm these data, we performed qRT-PCR analysis of the same specimens and showed that IDO1 transcripts levels were 13-fold lower ($p = 0.0003$) in treated animals compared with controls (Figure 3J). Similar experiments in CT2A-bearing mice showed little alteration in intratumoral IDO1 levels (Figures 3K and 3L).

PPRX-1701 treatment alters the cellular immune composition of the tumor microenvironment

Because PPRX-1701 may affect multiple immune modulators (Figure 1) and IDO1 is known to contribute to the immunosuppressive phenotype of the GBM TME,[26,31,32] we examined the composition of the infiltrating immune cells after PPRX-1701 treatment. To do this, we treated mice bearing GL261 tumors with a similar treatment regime to that described above (Figure 4A) and isolated tumor-infiltrating $CD45^+$ immune cells on day 29–30 after tumor implantation. To analyze the tumor-infiltrating cells, we used mass cytometry (CyTOF), which allows detailed analysis of immune cell composition. The marker panel is described in Table S1.

Using dimensional reduction analysis, we found that the GL261 TME contains 8 defined immune subpopulations as shown on the t-distributed stochastic neighbor embedding (tSNE) plot in Figure 4B. These data are similar to those obtained in previous phenotypic characterization of the TME in this model[33] and show the proportional presence of different immune cell metaclusters such as B cells, myeloid-derived suppressor cells (MDSCs), $CD8^+$ T cells, $CD4^+$ T cells, natural killer (NK) cells, and macrophages (Figure 4C).

Further analysis of the specimens from the PPRX-1701-treated group revealed significant global alterations in the TME (Figure 4D). Notably, there was a significant increase in the proportion of $CD8^+$ T cells ($p = 0.0006$) (Figure 4E). We also observed an increase in the subpopulation of $CD103^+$ dendritic cells ($p = 0.007$) usually associated with an effective $CD8^+$ T cell anti-tumor response.[34] Additionally, we noted a decrease in pro-tumor M2 macrophages ($p = 0.0075$) and increased numbers of $CD4^+$ T cells ($p = 0.0061$) in PPRX-1701-treated animals. These cells are known for their contribution to anti-tumor responses by coordinating antigen-specific immunity through their high plasticity and cytokine-producing ability.[35] We also noted a small elevation in the number of regulatory T cells in the TME of treated animals, which are usually associated with the poor prognosis in GBM[36,37]; however, this increase of 5.5% regulatory T cells (T-regs) in the total $CD45^+$ tumor-infiltrating lymphocyte (TIL) population in treated animals was not substantial amid other perturbations in TME of the treated animals and would likely not have a significant impact on anti-tumor response. Along with these changes, we also noted a decreased number of peritumoral B cells: 4% in control versus 2% of total tumor-infiltrating immune cells in treated animals ($p = 0.0013$). In terms of MDSCs, there was no change in the levels of monocytic-MDSCs but a trend toward reduction of polymorphonuclear-MDSCs in these data (Figure 4E).

Collectively, these results suggest that treatment with PPRX-1701 induces changes in the TME, which may enable anti-tumor responses via increased populations of cytotoxic $CD8^+$ T cells and supportive $CD103^+$ dendritic cells (DCs) and decreased numbers of pro-tumor macrophages and B cells. Overall, our data support the further development of PPRX-1701 as an agent

(G) BiA reaches intracranial tumors in murine GBM models after PPRX-1701 injection. G9 cells were stably transduced with TOPFlash and implanted intracranially in nude mice. Mice were scanned for luminescence 1 h after intravenous (i.v.) injection of PPRX-1701 (10 mg/kg).
(H) Mass spectrometry analysis of BiA concentration in a GL261 brain/tumor tissue and plasma after i.v. administration of PPRX-1701.
Data are represented as mean ± SD of at least three replicates.

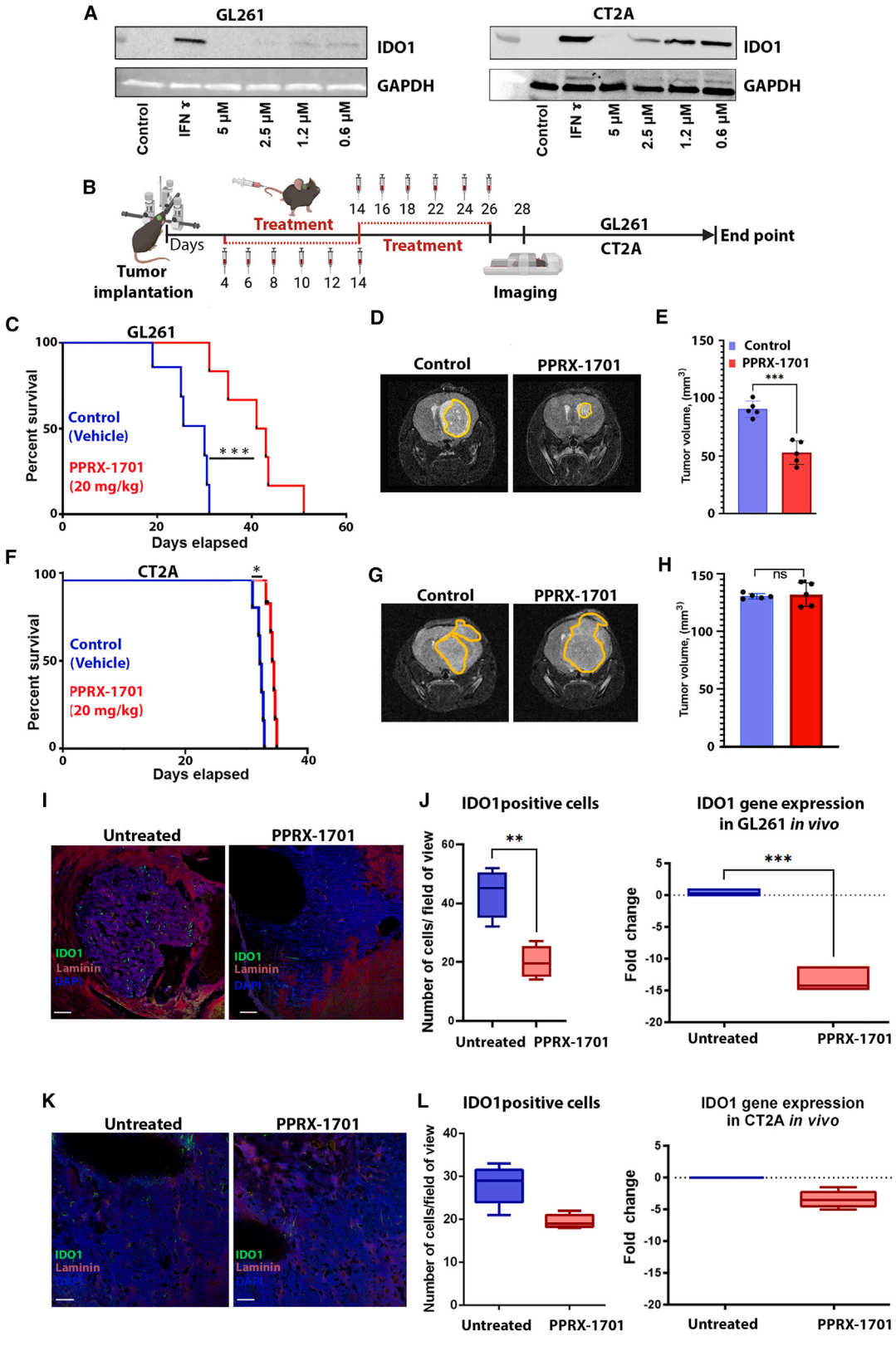

(legend on next page)

to facilitate treatment of GBM by multiple effects, including promotion of an anti-tumor immune environment.

DISCUSSION

Here, we show that BiA can impact expression of important immunoregulatory genes in GBM. Delivery of BiA using PPRX-1701 in mouse models impacted cell signaling pathways in intracranial tumors, altered the TME, and improved animal survival. The data support further development of this approach.

Our previous studies showed that BiA can extend survival of mice bearing orthotopic GBM xenografts.[19] We showed in these studies that BiA could impact the key cancer hallmarks of proliferation, angiogenesis, and invasion. Mechanistically, BiA is a small-molecule ATP-mimetic kinase inhibitor with a broad specificity. Key targets include JAK, GSK-3, cyclin-dependent, and Src family kinases. BiA is a chemical derivative of the traditional Chinese medicine indirubin, which has been used to treat leukemia and as a topical treatment for psoriasis.[20]

GBM is an aggressive cancer for which there are no effective treatments. The profound immunosuppressive TME of these tumors is an obstacle for the application of existing immunotherapies for treatment of GBM. Therefore, development of new therapeutics to manipulate the immune system to promote anti-tumor immunity in GBM is important. Here, we initially found that BiA can reduce the levels of key immunosuppressive proteins in GBM. Transcriptome profiling of GBM cells treated with the closely related compound BIO uncovered a cluster of 28 downregulated genes responsible for tumor–immune cell interactions. These differentially expressed genes include IDO1, a known immunosuppressive target in GBM and other cancers.[38–41] While enzymatic activity of IDO1 in GBM leads to the conversion of tryptophan into downstream immunosuppressive kynurenine, it is generally not expressed at appreciable levels in the adult central nervous system. However, its expression is rapidly stimulated by IFNγ, as one of the key mediators of immunological events in the tumor microenviroment.[42,43] Thus, validation of the inhibitory effect of BiA on IDO1 was of particular interest. In our *in vitro* studies, we showed that BiA induces sensitivity of the tumor cells toward T cell-mediated killing. To further validate these findings *in vivo*, we employed PPRX-1701, a previously untested formulation of BiA that facilitates systemic delivery via tail-vein injection at therapeutic concentrations.

Our preclinical trials led to the following important findings: (1) PPRX-1701 dosage at 20 mg/kg was readily achievable, with no discernable negative effects on mice; (2) BiA was able to reach its intracranial tumor target, as shown by a transcriptional reporter assay and mass spectrometry-based PK studies; (3) significantly longer survival of the immunocompetent GBM tumor models treated with PPRX-1701; (4) tumors from treated mice showed significantly lower expression of IDO1; and (5) in-depth high-dimensional mass cytometry revealed that the TME of the mice treated with PPRX-1701 was altered to potentially favor anti-tumor immunity, including increased $CD8^+$ T cells and decreased M2 macrophages. These data set the stage for future studies to determine maximum levels and dosing of PPRX-1701. Additional mouse GBM models and therapeutic combinations with standard of care and immune checkpoint blockade will be performed to provide support for this approach. Future studies will also examine the combination with standard-of-care therapies (chemotherapy and irradiation), which will be valuable for further translational studies and clinical evaluation. Inhibition of IDO1 may allow BiA to play the role of an efficient sensitizer for radiation therapy and may also enhance efficacy of immunotherapy by shaping the TME toward a local immune response in immunologically resistant recurrent tumors.[44] In this regard, it would be also important to test this approach in immunologically "cold" tumor models such as CT2A, as it was already shown that inhibition of IDO1 synergizes with chemoradiation therapy to enhance survival in the GL261 GBM model.[44] However, this hypothesis needs to be carefully investigated in our future preclinical studies.

While our entire preclinical *in vivo* assessment of BiA/PPRX was performed on female mice, it is important to mention that observed immunological phenotypes in GBM may differ by gender according to recent evidence.[45,46] According to these studies, gender differences might also dictate different trajectories for immunological responses in male and female patients, mostly driven by the immunosuppressive myeloid population in the TME, potentially associated with influence of sex hormones on the immune response.

In summary, the data presented in this work identify PPRX-1701/BiA as a potential drug candidate that could boost existing immunotherapeutic approaches in GBM. We were able to show that PPRX-1701 is a promising agent with the potential to target multiple hallmarks of GBM including tumor immune interactions.

Limitations of the study

The efficacy of PPRX-1701 is shown using the common preclinical murine GBM models GL261 and CT2A, which are known as relatively immunologically "hot" and "cold" models,

Figure 3. BiA/PPRX-1701 inhibits IDO1 expression and prolongs survival in mouse GBM

(A) Validation of BiA inhibition of IDO1 induction in mouse GL261 and CT2A GBM cells. Cells were stimulated with 100 ng/mL IFNγ for 24 h ± BiA at different concentrations.

(B) Outline of *in vivo* experimental setup. 50,000 GL261 or CT2A cells were injected intracranially in the right hemisphere; treatment was started on day 14 for GL261 and day 4 for CT2A model after tumor implantation. PPRX-1701 was administered i.v. for a total of 6 doses 3 times per week.

(C–H) Survival of tumor-bearing mice. As shown in (C)'s Kaplan-Meier survival curve, treatment with PPRX-1701 (42 days) led to a significant increase in median survival compared with control (30 days) (PPRX-1701 versus control; log rank test: $p = 0.0006$) To compare tumor size, T2-weighted MRI images were acquired 28 days after tumor implantation. Representative images are shown in (D). All treated animals ($n = 5$/group) displayed smaller tumor volume as shown (E). Data are represented as mean ± SD ($p < 0.0001$). As shown in (F), treatment with PPRX-1701 led to small but significant difference in survival of CT2A tumor-bearing mice.

(I–L) IDO1 expression in GL261 and CT2A tumor tissue *in vivo* assessed by immunofluorescence (scale bar: 200 μm) and shows a significant reduction in the number of $IDO1^+$ cells in a tumor mass as quantified and showed on bar graphs. This correlates with transcriptional level of IDO1 in the tumor mass assessed by qPCR analysis as shown on the bar graphs (J and L) ($p < 0.001$).

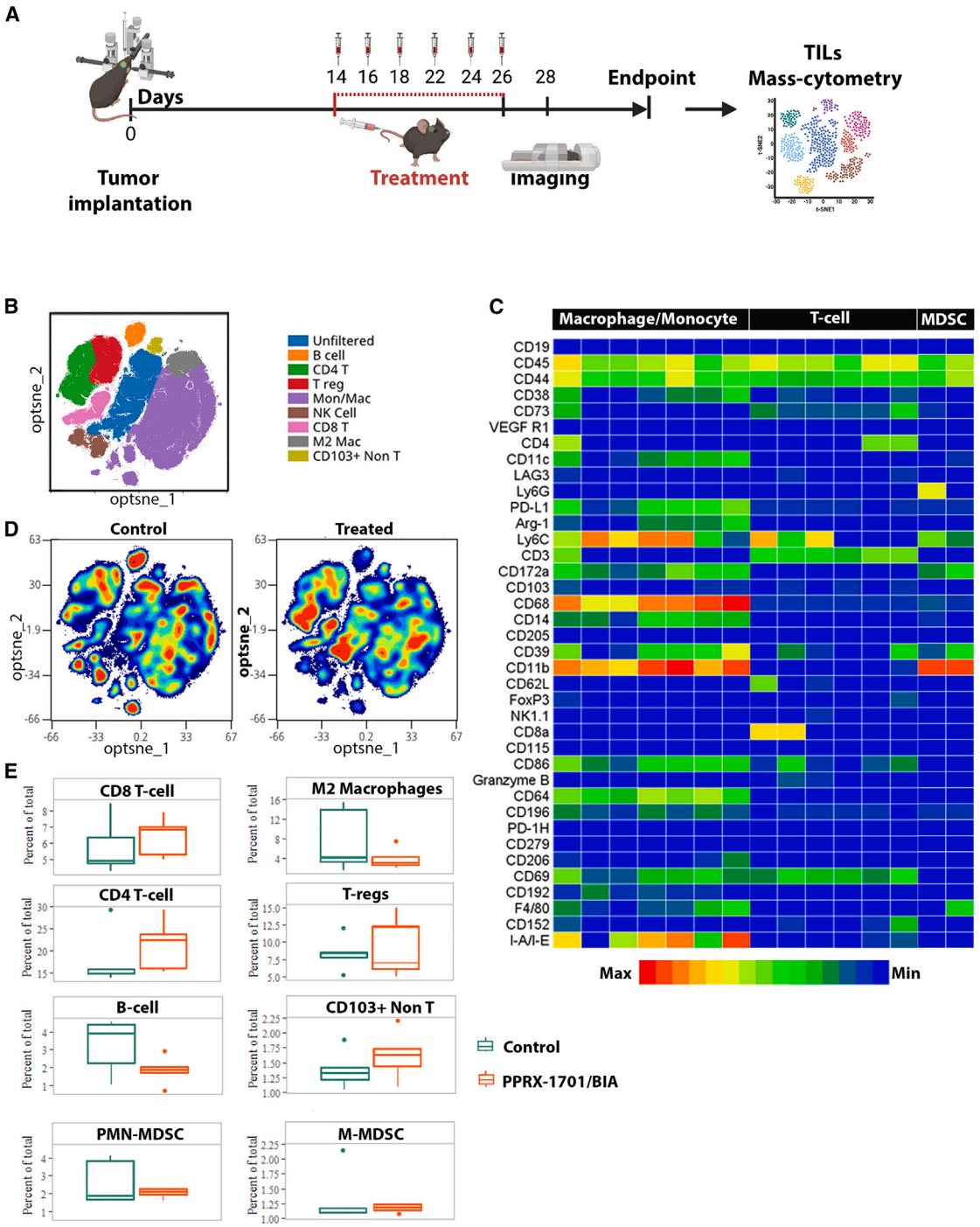

Figure 4. Treatment with BiA-PPRX-1701 impacts the GL261 tumor microenvironment

(A) Experimental outline: 50,000 GL261 cells were injected intracranially, and PPRX-1701 treatment was started on day 14 after tumor implantation. Tumor-infiltrating lymphocytes were isolated from endpoint mice from both groups and analyzed by mass cytometry (CyTOF).

(B) Concatenated tSNE plot of all samples showing metaclusters of various populations of immune cells in the TME defined by expression analysis (n = 4 mice/group).

(C) Heatmap represents expression profile of metaclusters in concatenated samples significantly altered after PPRX-1701 treatment. Heatmap displaying marker expression in the leukocyte clusters.

(D) tSNE plots showing differences between PPRX-1701-treated and control groups.

(E) Bar plots represent levels of significantly altered tumor-infiltrating lymphocyte (TIL) subpopulations in animals treated with PPRX-1701 compared with untreated controls.

respectively. These models were specifically chosen based on their well-described immunogenic profile but are not genetically typical of GBM. Our experimental strategy was used to highlight the potential importance of IDO1. Further studies employing genetically engineered GBM mouse models (GEMMs) and transgenic mice would be important to further support these observations. However, together with the presented models in this study, this approach will be an important part of the complete preclinical validation prior to further steps toward testing PPRX-1701 in clinical trials.

STAR★METHODS

Detailed methods are provided in the online version of this paper and include the following:

- KEY RESOURCES TABLE
- RESOURCE AVAILABILITY
  - Lead contact
  - Materials availability
  - Data and code availability
- EXPERIMENTAL MODEL AND SUBJECT DETAILS
  - Mice
  - Cell lines
- METHOD DETAILS
  - Microarray analysis
  - PPRX-1701 preparation details
  - Cell treatments
  - T cell cytotoxicity assay
  - Immunoblot analysis
  - *In vitro* cell proliferation assays
  - *In vitro* cell migration assays
  - Quantitative real-time PCR analysis
  - *In vivo* studies
  - MRI imaging
  - Immunohistochemistry
  - Isolation of murine tumor-infiltrating leukocytes
  - Mass cytometry (CyTOF)
  - Quantification of 6′-bromoindirubin-3′ acetoxime
  - Hematoxylin & eosin (H&E) staining of murine liver and spleen sections
- QUANTIFICATION AND STATISTICAL ANALYSIS

SUPPLEMENTAL INFORMATION

Supplemental information can be found online at https://doi.org/10.1016/j.xcrm.2023.101019.

ACKNOWLEDGMENTS

This work was supported by NCI grants RO1CA166172 (E.A.C.), R50-CA243706 (M.O.N.), and R21CA259734 (S.E.L.). The Thermo LC Orbitrap MS was supported by a National Science Foundation MRI award (1919870, K.D.P.) and the NIEHS Training in Environmental Pathology T32 program T32ES007272 (K.E.M.).

AUTHOR CONTRIBUTIONS

Conceptualization, M.Z. and S.E.L.; formal analysis, M.Z., A.L.L., R.P., and K.E.M.; methodology, M.Z., M.O.N., and S.E.L.; investigation, M.Z., J.-L.J.-M., M.O.N., M.S.K., T.F., K.E.M., and K.D.P.; resources, B.W., Y.T., P.B., and W.L.; writing – original draft, M.Z. and S.E.L.; writing – review & editing, M.Z. and S.E.L.; visualization, M.Z.; supervision, E.A.C., and S.E.L.; funding acquisition, E.A.C. and S.E.L.

DECLARATION OF INTERESTS

B.W., P.B., Y.T., and W.Y. have been employees of Phosphorex, Inc. B.W. is also an employee of Cytodigm, Inc. The development of deliverable nanoparticles of indirubin is disclosed in patent CA2914782C "Nanoparticles of indirubin, derivatives thereof and methods of making and using same" Phosphorex, Inc.

INCLUSION AND DIVERSITY

We support inclusive, diverse, and equitable conduct of research.

Received: April 7, 2022
Revised: December 22, 2022
Accepted: March 21, 2023
Published: April 14, 2023

REFERENCES

1. Filbin, M.G., and Suvà, M.L. (2016). Gliomas genomics and epigenomics: arriving at the start and knowing it for the first time. Annu. Rev. Pathol. *11*, 497–521. https://doi.org/10.1146/annurev-pathol-012615-044208.
2. Alexander, B.M., and Cloughesy, T.F. (2017). Adult glioblastoma. J. Clin. Oncol. *35*, 2402–2409. https://doi.org/10.1200/JCO.2017.73.0119.
3. Aldape, K., Brindle, K.M., Chesler, L., Chopra, R., Gajjar, A., Gilbert, M.R., Gottardo, N., Gutmann, D.H., Hargrave, D., Holland, E.C., et al. (2019). Challenges to curing primary brain tumours. Nat. Rev. Clin. Oncol. *16*, 509–520. https://doi.org/10.1038/s41571-019-0177-5.
4. Hottinger, A.F., Abdullah, K.G., and Stupp, R. (2016). Current standards of care in glioblastoma therapy. Glioblastoma (Elsevier Inc.), pp. 73–80. https://doi.org/10.1016/B978-0-323-47660-7.00006-95.
5. Stupp, R., Mason, W.P., Van Den Bent, M.J., Weller, M., Fisher, B., Taphoorn, M.J.B., Belanger, K., Brandes, A.A., Marosi, C., Bogdahn, U., et al. (2005). Radiotherapy plus concomitant and adjuvant temozolomide for glioblastoma. N. Engl. J. Med. *352*, 987–996. https://doi.org/10.1056/NEJMoa043330.
6. Snyder, A., Makarov, V., Merghoub, T., Yuan, J., Zaretsky, J.M., Desrichard, A., Walsh, L.A., Postow, M.A., Wong, P., Ho, T.S., et al. (2014). Genetic basis for clinical response to CTLA-4 blockade in melanoma. N. Engl. J. Med. *371*, 2189–2199. https://doi.org/10.1056/NEJMoa1406498.
7. Perez-Gracia, J.L., Labiano, S., Rodriguez-Ruiz, M.E., Sanmamed, M.F., and Melero, I. (2014). Orchestrating immune check-point blockade for cancer immunotherapy in combinations. Curr. Opin. Immunol. *27*, 89–97. https://doi.org/10.1016/j.coi.2014.01.002.
8. Topalian, S.L., Drake, C.G., and Pardoll, D.M. (2015). Immune checkpoint blockade: a common denominator approach to cancer therapy. Cancer Cell *27*, 450–461. https://doi.org/10.1016/j.ccell.2015.03.001.
9. Wei, S.C., Duffy, C.R., and Allison, J.P. (2018). Fundamental mechanisms of immune checkpoint blockade therapy. Cancer Discov. *8*, 1069–1086. https://doi.org/10.1158/2159-8290.CD-18-0367.
10. Tomaszewski, W., Sanchez-Perez, L., Gajewski, T.F., and Sampson, J.H. (2019). Brain tumor microenvironment and host state: implications for immunotherapy. Clin. Cancer Res. *25*, 4202–4210. https://doi.org/10.1158/1078-0432.CCR-18-1627.
11. Sena, I.F.G., Paiva, A.E., Prazeres, P.H.D.M., Azevedo, P., Lousado, L., Bhutia, S.K., Salmina, A.B., Mintz, A., and Lousado, L. (2018). Glioblastoma-activated pericytes support tumor growth via immunosuppression. Cancer Med. *7*, 1232–1239. https://doi.org/10.1002/cam4.1375.

12. Chen, Z., and Hambardzumyan, D. (2018). Immune microenvironment in glioblastoma subtypes. Front. Immunol. *9*, 1004. https://doi.org/10.3389/fimmu.2018.01004.

13. Gabriely, G., Wheeler, M.A., Takenaka, M.C., and Quintana, F.J. (2017). Role of AHR and HIF-1α in glioblastoma metabolism. Trends Endocrinol. Metab. *28*, 428–436. https://doi.org/10.1016/j.tem.2017.02.009.

14. Zhong, S., Jeong, J.H., Chen, Z., Chen, Z., and Luo, J.L. (2020). Targeting tumor microenvironment by small-molecule inhibitors. Transl. Oncol. *13*, 57–69. https://doi.org/10.1016/j.tranon.2019.10.001.

15. Weller, M., Roth, P., Preusser, M., Wick, W., Reardon, D.A., Platten, M., and Sampson, J.H. (2017). Vaccine-based immunotherapeutic approaches to gliomas and beyond. Nat. Rev. Neurol. *13*, 363–374. https://doi.org/10.1038/nrneurol.2017.64.

16. Klemm, F., Maas, R.R., Bowman, R.L., Kornete, M., Soukup, K., Nassiri, S., Brouland, J.P., Iacobuzio-Donahue, C.A., Brennan, C., Tabar, V., et al. (2020). Interrogation of the microenvironmental landscape in brain tumors reveals disease-specific alterations of immune cells. Cell *181*, 1643–1660.e17. https://doi.org/10.1016/j.cell.2020.05.007.

17. Friebel, E., Kapolou, K., Unger, S., Núñez, N.G., Utz, S., Rushing, E.J., Regli, L., Weller, M., Greter, M., Tugues, S., et al. (2020). Single-cell mapping of human brain cancer reveals tumor-specific instruction of tissue-invading leukocytes. Cell *181*, 1626–1642.e20. https://doi.org/10.1016/j.cell.2020.04.055.

18. Tamura, R., Tanaka, T., Akasaki, Y., Murayama, Y., Yoshida, K., and Sasaki, H. (2019). The role of vascular endothelial growth factor in the hypoxic and immunosuppressive tumor microenvironment: perspectives for therapeutic implications. Med. Oncol. *37*, 2. https://doi.org/10.1007/s12032-019-1329-2.

19. Williams, S.P., Nowicki, M.O., Liu, F., Press, R., Godlewski, J., Abdel-Rasoul, M., Kaur, B., Fernandez, S.A., Chiocca, E.A., and Lawler, S.E. (2011). Indirubins decrease glioma invasion by blocking migratory phenotypes in both the tumor and stromal endothelial cell compartments. Cancer Res. *71*, 5374–5380. https://doi.org/10.1158/0008-5472.CAN-10-3026.

20. Blažević, T., Heiss, E.H., Atanasov, A.G., Breuss, J.M., Dirsch, V.M., and Uhrin, P. (2015). Indirubin and indirubin derivatives for counteracting proliferative diseases. eCAM. https://doi.org/10.1155/2015/654098.

21. Wang, X.G., and Liu, Z.J. (2014). Prevention and treatment of viral respiratory infections by traditional Chinese herbs. Chin. Med. J. (Engl.) *127*, 1344–1350. https://doi.org/10.3760/cma.j.issn.0366-6999.20132029.

22. Perabo, F.G.E., Frössler, C., Landwehrs, G., Schmidt, D.H., von Rücker, A., Wirger, A., and Müller, S.C. (2006). Indirubin-3'-monoxime, a CDK inhibitor induces growth inhibition and apoptosis-independent up-regulation of survivin in transitional cell cancer. Anticancer Res. *26*, 2129–2135.

23. Babcock, A.S., Anderson, A.L., and Rice, C.D. (2013). Indirubin-3'-(2,3 dihydroxypropyl)-oximether (E804) is a potent modulator of LPS-stimulated macrophage functions. Toxicol. Appl. Pharmacol. *266*, 157–166. https://doi.org/10.1016/j.taap.2012.10.011.

24. Nam, S., Buettner, R., Turkson, J., Kim, D., Cheng, J.Q., Muehlbeyer, S., Hippe, F., Vatter, S., Merz, K.H., Eisenbrand, G., and Jove, R. (2005). Indirubin derivatives inhibit Stat3 signaling and induce apoptosis in human cancer cells. Proc. Natl. Acad. Sci. USA *102*, 5998–6003. https://doi.org/10.1073/pnas.0409467102.

25. Eldar-Finkelman, H., and Martinez, A. (2011). GSK-3 inhibitors: preclinical and clinical focus on CNS. Front. Mol. Neurosci. *4*, 32. https://doi.org/10.3389/fnmol.2011.00032.

26. Zhai, L., Bell, A., Ladomersky, E., Lauing, K.L., Bollu, L., Sosman, J.A., Zhang, B., Wu, J.D., Miller, S.D., Meeks, J.J., et al. (2020). Immunosuppressive Ido in cancer: mechanisms of action, animal models, and targeting strategies. Front. Immunol. *11*, 1185. https://doi.org/10.3389/fimmu.2020.01185.

27. Mineo, M., Lyons, S.M., Zdioruk, M., von Spreckelsen, N., Ferrer-Luna, R., Ito, H., Alayo, Q.A., Kharel, P., Giantini Larsen, A., Fan, W.Y., et al. (2020). Tumor interferon signaling is regulated by a lncRNA INCR1 transcribed from the PD-L1 locus. Mol. Cell *78*, 1207–1223.e8. https://doi.org/10.1016/j.molcel.2020.05.015.

28. Sussman, D.J. (2002). LEF/TCF-dependent, fluorescence-based reporter gene assay for Wnt signaling. Biotechniques *32*, 1000–1002. https://doi.org/10.2144/02325bm04.

29. Kramer, T., Schmidt, B., and Lo Monte, F. (2012). Small-molecule inhibitors of GSK-3: structural insights and their application to Alzheimer's disease models. Int. J. Alzheimer's Dis. *2012*, 381029. https://doi.org/10.1155/2012/381029.

30. Ladomersky, E., Zhai, L., Lauing, K.L., Bell, A., Xu, J., Kocherginsky, M., Zhang, B., Wu, J.D., Podojil, J.R., Platanias, L.C., et al. (2020). Advanced age increases immunosuppression in the brain and decreases immunotherapeutic efficacy in subjects with glioblastoma. Clin. Cancer Res. *26*, 5232–5245. https://doi.org/10.1158/1078-0432.CCR-19-3874.

31. Ozawa, Y., Yamamuro, S., Sano, E., Tatsuoka, J., Hanashima, Y., Yoshimura, S., Sumi, K., Hara, H., Nakayama, T., Suzuki, Y., and Yoshino, A. (2020). Indoleamine 2,3-dioxygenase 1 is highly expressed in glioma stem cells. Biochem. Biophys. Res. Commun. *524*, 723–729. https://doi.org/10.1016/j.bbrc.2020.01.148.

32. Labadie, B.W., Bao, R., and Luke, J.J. (2019). Reimagining Ido pathway inhibition in cancer immunotherapy via downstream focus on the tryptophan–kynurenine–aryl hydrocarbon axis. Clin. Cancer Res. *25*, 1462–1471. https://doi.org/10.1158/1078-0432.CCR-18-2882.

33. Khalsa, J.K., Cheng, N., Keegan, J., Chaudry, A., Driver, J., Bi, W.L., Lederer, J., and Shah, K. (2020). Immune phenotyping of diverse syngeneic murine brain tumors identifies immunologically distinct types. Nat. Commun. *11*, 3912. https://doi.org/10.1038/s41467-020-17704-5.

34. Gardner, A., de Mingo Pulido, Á., and Ruffell, B. (2020). Dendritic cells and their role in immunotherapy. Front. Immunol. *11*, 924. https://doi.org/10.3389/fimmu.2020.00924.

35. Wang, H., Zhou, H., Xu, J., Lu, Y., Ji, X., Yao, Y., Chao, H., Zhang, J., Zhang, X., Yao, S., et al. (2021). Different T-cell subsets in glioblastoma multiforme and targeted immunotherapy. Cancer Lett. *496*, 134–143. https://doi.org/10.1016/j.canlet.2020.09.028.

36. Humphries, W., Wei, J., Sampson, J.H., and Heimberger, A.B. (2010). The role of tregs in glioma-mediated immunosuppression: potential target for intervention. Neurosurg. Clin. N. Am. *21*, 125–137. https://doi.org/10.1016/j.nec.2009.08.012.

37. Woroniecka, K.I., Rhodin, K.E., Chongsathidkiet, P., Keith, K.A., and Fecci, P.E. (2018). T-cell dysfunction in glioblastoma: applying a new framework. Clin. Cancer Res. *24*, 3792–3802. https://doi.org/10.1158/1078-0432.CCR-18-0047.

38. Prendergast, G.C., Malachowski, W.J., Mondal, A., Scherle, P., and Muller, A.J. (2018). Indoleamine 2,3-dioxygenase and its therapeutic inhibition in cancer. Int. Rev. Cell Mol. Biol. *336*, 175–203. https://doi.org/10.1016/bs.ircmb.2017.07.004.

39. Platten, M., von Knebel Doeberitz, N., Oezen, I., Wick, W., and Ochs, K. (2014). Cancer immunotherapy by targeting Ido1/TDO and their downstream effectors. Front. Immunol. *5*, 673. https://doi.org/10.3389/fimmu.2014.00673.

40. Ladomersky, E., Zhai, L., Lenzen, A., Lauing, K.L., Qian, J., Scholtens, D.M., Gritsina, G., Sun, X., Liu, Y., Yu, F., et al. (2018). Ido1 inhibition synergizes with radiation and PD-1 blockade to durably increase survival against advanced glioblastoma. Clin. Cancer Res. *24*, 2559–2573. https://doi.org/10.1158/1078-0432.CCR-17-3573.

41. Cheong, J.E., and Sun, L. (2018). Targeting the Ido1/TDO2–KYN–AhR pathway for cancer immunotherapy – challenges and opportunities. Trends Pharmacol. Sci. *39*, 307–325. https://doi.org/10.1016/j.tips.2017.11.007.

42. Zhai, L., Ladomersky, E., Dostal, C.R., Lauing, K.L., Swoap, K., Billingham, L.K., Gritsina, G., Wu, M., McCusker, R.H., Binder, D.C., and Wainwright, D.A. (2017). Non-tumor cell Ido1 predominantly contributes to enzyme activity and response to CTLA-4/PD-L1 inhibition in mouse glioblastoma.

Brain Behav. Immun. *62*, 24–29. https://doi.org/10.1016/j.bbi.2017.01.022.

43. Hosseinalizadeh, H., Mahmoodpour, M., Samadani, A.A., and Roudkenar, M.H. (2022). The immunosuppressive role of indoleamine 2, 3-dioxygenase in glioblastoma: mechanism of action and immunotherapeutic strategies. Med. Oncol. *39*, 130. https://doi.org/10.1007/s12032-022-01724-w.

44. Li, M., Bolduc, A.R., Hoda, M.N., Gamble, D.N., Dolisca, S.B., Bolduc, A.K., Hoang, K., Ashley, C., McCall, D., Rojiani, A.M., et al. (2014). The indoleamine 2,3-dioxygenase pathway controls complement-dependent enhancement of chemo-radiation therapy against murine glioblastoma. J. Immunother. Cancer *2*, 21. https://doi.org/10.1186/2051-1426-2-21.

45. Bayik, D., Zhou, Y., Park, C., Hong, C., Vail, D., Silver, D.J., Lauko, A., Roversi, G., Watson, D.C., Lo, A., et al. (2020). Myeloid-derived suppressor cell subsets drive glioblastoma growth in a sex-specific manner. Cancer Discov. *10*, 1210–1225. https://doi.org/10.1158/2159-8290.CD-19-1355.

46. Lee, J., Kay, K., Troike, K., Ahluwalia, M.S., and Lathia, J.D. (2022). Sex differences in glioblastoma immunotherapy response. Neuromolecular Med. *24*, 50–55. https://doi.org/10.1007/s12017-021-08659-x.

47. Stevens, M.M., Maire, C.L., Chou, N., Murakami, M.A., Knoff, D.S., Kikuchi, Y., Kimmerling, R.J., Liu, H., Haidar, S., Calistri, N.L., et al. (2016). Drug sensitivity of single cancer cells is predicted by changes in mass accumulation rate. Nat. Biotechnol. *34*, 1161–1167. https://doi.org/10.1038/nbt.3697.

48. Finck, R., Simonds, E.F., Jager, A., Krishnaswamy, S., Sachs, K., Fantl, W., Pe'er, D., Nolan, G.P., and Bendall, S.C. (2013). Normalization of mass cytometry data with bead standards. Cytometry A. *83*, 483–494. https://doi.org/10.1002/cyto.a.22271.

49. Chevrier, S., Crowell, H.L., Zanotelli, V.R.T., Engler, S., Robinson, M.D., and Bodenmiller, B. (2018). Compensation of signal spillover in suspension and imaging mass cytometry. Cell Syst. *6*, 612–620.e5. https://doi.org/10.1016/j.cels.2018.02.010.

50. Zunder, E.R., Finck, R., Behbehani, G.K., Amir, E.A.D., Krishnaswamy, S., Gonzalez, V.D., Lorang, C.G., Bjornson, Z., Spitzer, M.H., Bodenmiller, B., et al. (2015). Palladium-based mass tag cell barcoding with a doublet-filtering scheme and single-cell deconvolution algorithm. Nat. Protoc. *10*, 316–333. https://doi.org/10.1038/nprot.2015.020.

51. Chu, G., Li, J., Narasimhan, B., Tibshirani, R., and Tusher, V. (2001). SAM - Significance Analysis of Microarrays - Users guide and technical document. Policy [Internet]. http://groups.yahoo.com/group/sam-software.

52. MacDougall, D., and Crummett, W.B. (1980). Guidelines for data acquisition and data quality evaluation in environmental chemistry. Anal. Chem. *52*, 2242–2249. https://doi.org/10.1021/ac50064a004.

STAR★METHODS

KEY RESOURCES TABLE

REAGENT or RESOURCE	SOURCE	IDENTIFIER
Antibodies		
Anti-IDO (human)	Cell Signaling Technology	Cat# 86630; RRID: AB_2636818
Anti-IDO (mouse)	Cell Signaling Technology	Cat#51851; RRID: AB_2799402
Alexa Fluor 488 AffiniPure Donkey Anti-Rabbit IgG	Jackson ImmunoResearch	Cat# 711-545-152; RRID: AB_2313584
Alexa Fluor 594 AffiniPure Donkey Anti-Rabbit IgG	Jackson ImmunoResearch	Cat# 711-545-152; RRID: AB_2340621
Alexa Fluor 647 AffiniPure Donkey Anti-Rabbit IgG	Jackson ImmunoResearch	Cat# 711-545-152; RRID: AB_2492288
Anti-GAPDH (D16H11)	Cell Signaling Technology	Cat#51332; RRID: AB_2799390
Chemicals, peptides, and recombinant proteins		
Recombinant Human IFN-γ	PeproTech	Cat# 300-02
RIPA buffer	Thermo Fisher Scientific	Cat# J62524.AE
cOmplete™, Mini, EDTA-free Protease Inhibitor Cocktail	Sigma Millipore	Cat# 11836170001
Formalin solution, neutral buffered, 10%	Sigma-Aldrich	Cat# HT501128
VECTASHIELD® Hardset Antifade Mounting Medium	Vector Laboratories	Cat# EW-93952-27
Sucrose	Sigma-Aldrich	Cat#57-50-1
Type I Collagen Solution, PureCol®	Advanced Biomatrix	Cat#5005
B-27™ Supplement	Thermo Fisher Scientific	Cat#17504044
Recombinant Human FGF	PeproTech	Cat#100-18B
Recombinant Human EGF	PeproTech	Cat#GMP100-15
Bradford Dye Reagent	BioRad	Cat# 5000205
Trizol	Thermo Fisher Scientific	Cat# 15596018
Critical commercial assays		
Lipofectamine 2000	Thermo Fisher Scientific	Cat# 11668019
Hematoxylin & Eosin Stain Kit	Vector Laboratories	Cat# H-3502
iScript cDNA Synthesis kit	Bio-Rad	Cat# 1708891
Power SYBR Green PCR Master Mix	Thermo Fisher Scientific	Cat# 4368577
RNeasy Mini Kit	QIAGEN	Cat# 74104
Dynabeads Human T-Activator	Thermo Fisher Scientific	Cat# 11161D
Muse Count & Viability Kit	Millipore	Cat# MCH100102
Annexin V-FITC Apoptosis Staining/Detection Kit	Abcam	Cat# ab14085
Ficoll Paque Plus	GE Healthcare	Cat# 17-1440-02
$CD8^+$ T cell Isolation Kit, human	Miltenyi Biotec	Cat# 130-096-495
EasySep Human T cell Isolation Kit	StemCell Technologies, Inc.	Cat# 17951
Tumor Dissociation Kit, mouse	Miltenyi Biotec	Cat# 130-096-730
Netwell® inserts	Corning	Cat# 3480
Experimental models: Cell lines		
Human: U251 cells	NCI-DTP	Cat# U-251; RRID: CVCL_0021
Human: G9 cells	OSU Ohio	
Human: G68 cells	OSU Ohio	
Human: G34 cells	OSU Ohio	
Mouse: GL261fluc2	PerkinElmer	BW134246
Mouse: CT2A	Boston College	
Deposited data		
Data from transcriptomic microarray analysis	ArrayExpress	Array Express: E-MTAB-12775

(*Continued on next page*)

Continued

REAGENT or RESOURCE	SOURCE	IDENTIFIER
Experimental models: Organisms/strains		
C57BL/6J Mice	The Jackson Laboratory	000664
Software and algorithms		
Fiji - ImageJ	https://imagej.net/Fiji	RRID: SCR_002285
FlowJo	https://www.flowjo.com	RRID: SCR_008520
Graphpad prism version 8	https://www.graphpad.com/scientific-software/prism/	RRID: SCR_002798
ZEN Digital Imaging for Light Microscopy	https://www.zeiss.com/microscopy/en_us/products/microscope-software/zen.html	RRID: SCR_013672

RESOURCE AVAILABILITY

Lead contact

Further information and requests for resources and reagents should be directed to and will be fulfilled by the lead contact, Sean E. Lawler (sean_lawler@brown.edu).

Materials availability

All unique reagents generated in this study are available from the lead contact with a completed material transfer agreement.

Data and code availability

The datasets generated during this study have been deposited at Array Express (EBI-based functional genomics). Accession number is listed in the key resources table. This paper does not report original code. Any additional information required to reanalyze the data reported in this paper is available from the lead contact upon request.

EXPERIMENTAL MODEL AND SUBJECT DETAILS

Mice

Female C57/BL6 mice aged 8 and 28 weeks were used for the experiments and purchased from The Jackson Laboratory. Animals were maintained under pathogen-free conditions at the BWH Center for Comparative Medicine, Brigham and Women's Hospital. Mouse studies were conducted according to the protocols approved by the Institutional Animal Care and Use Committee (IACUC).

Cell lines

Patient-derived primary GBM cells were generated as described previously.[47] In detail, glioma tumors G9, G34, and G68 were collected with patient consent, according to the regulations of clinical trials and tissue procurement regulations of The Ohio State University. Tissue specimens were collected approximately 2 h post-surgery and immediately processed. The fragments of tumor tissue (0.1–2 g) were mechanically disrupted using Netwell mesh inserts and 3 mL syringe plungers (Corning) to achieve smaller, approximately 400 μm fragments. The obtained tissue fragments were then washed three times with Neurobasal medium (Thermo Fisher Scientific) supplemented with glutamine (Thermo Fisher Scientific), B27 (Thermo Fisher Scientific), 20 ng/mL epidermal growth factor (EGF), and fibroblast growth factor (FGF)-2 (PeproTech), and incubated in 20 mL of Neurobasal medium in 75 cm^2 flasks in a humidified 5% CO_2 incubator at 37°C. After 5–7 days, the cell aggregates were partially mechanically disrupted with a 1 mL pipette, and the cell suspension was washed with Neurobasal medium by spinning at 300 g for 5 min, followed by supernatant removal. The growth of the cell spheroids was followed for approximately 4–6 weeks until the growth medium was free of debris, and cellular aggregates had no internal debris accumulation.

U251 cells were obtained from the NCI-DTP and cultured in DMEM (Thermo Fisher Scientific) supplemented with 10% fetal bovine serum (FBS, Sigma-Aldrich), and 100 U/ml penicillin-streptomycin (Thermo Fisher Scientific). The cells were maintained in a humidified 5% CO_2 incubator at 37°C.

METHOD DETAILS

Microarray analysis

For transcriptomic studies a microarray was performed with Miltenyi Biotech (Germany), U251 cells (1 million cells in a 6 well dish) were treated with 5 μM BIO or vehicle (DMSO) controls. RNA was prepared using TRIzol reagent and RNA quality determined using an Agilent Bioanalyzer. Samples used all had an RNA Integrity number higher than 6.

100 ng total RNA from each sample was amplified and labeled with the Agilent Low Input Quick Amp Labeling Kit. Yields of cRNA and the dye-incorporation rate were measured with the ND-1000 Spectrophotometer (NanoDrop Technologies). The hybridization procedure was performed according to the Agilent 60-mer oligo microarray processing protocol using the Agilent Gene Expression Hybridization Kit (Agilent Technologies). Briefly, 600 ng Cy3-labeled fragmented cRNA in hybridization buffer was hybridized overnight (17 h, 65°C) to Agilent W hole Human Genome Oligo Microarrays 8 × 60K using Agilent's recommended hybridization chamber and oven. Finally, the microarrays were washed once with the Agilent Gene Expression Wash Buffer 1 for 1 min at room temperature followed by a second wash with preheated Agilent Gene Expression Wash Buffer 2 (37°C) for 1 min. Fluorescence signals of the hybridized Agilent Microarrays were detected using Agilent's Microarray Scanner System (Agilent Technologies). The Agilent Feature Extraction Software (FES) was used to readout and process the microarray image files. The software determines feature intensities (including background subtraction), rejects outliers and calculates statistical confidences. For determination of differential gene expression FES derived output data files were further analyzed using the Rosetta Resolver gene expression data analysis system (Rosetta Biosoftware).

PPRX-1701 preparation details

Preparation of PPRX-1701 was described previously (National Center for Biotechnology Information. "PubChem Patent Summary for US-2015110878-A1" PubChem, https://pubchem.ncbi.nlm.nih.gov/patent/US-2015110878-A1). Briefly, 6 mg of BiA and 50 mg of poly(ethylene glycol-co-lactide), AK31 (PolySciTech, West Lafayette, IN), were dissolved in 7 mL of dimethyl sulfoxide (DMSO) to result in a polymer-BiA solution, which was subsequently added dropwise to a beaker containing 50 mL of 1% by weight polyvinyl alcohol solution while stirring. The resulting nanoparticle suspension was washed 3 times with tangential flow filtration and concentrated to an appropriate percentage of particle content. Particle size analysis was performed with a Particle Size Analyzer (Malvern, Worcestershire, UK). The average particle size was found to be 165.2 nm. The BiA loading in PPRX-1701 was measured using HPLC and was found to be 4.5% by weight.

Cell treatments

siRNA induced IDO1 gene knock down was performed by transfecting G9 cells with 50 nM of predesigned siRNA (Thermo Fisher Scientific, AM16708, ID: 1107). Stimulation with IFNγ (PeproTech) was performed at 100 ng/mL IFNγ for a period of 24h.

T cell cytotoxicity assay

Peripheral blood mononuclear cells (PBMCs) were obtained from healthy human donors at the Harvard Crimson Blood Bank as approved by the IRB at the Brigham and Women's Hospital. PBMCs were isolated using Ficoll Plaque Plus (GE Healthcare Life Sciences) following the manufacturer's instructions. $CD8^+$ T cells were isolated by negative selection using the $CD8^+$ T cell Isolation Kit (Miltenyi Biotec). Isolation was performed according to the manufacturer's recommendations.

For 3D cytotoxicity assays, 750 GFP positive control or BiA/PPRX-1701 treated tumor cells were seeded in a round bottom low-attachment 96 well. Cells were allowed to form tumorspheres for 72h. After tumorspheres were formed, 2000 non-stimulated $CD8^+$ T cells or $CD8^+$ T cells stimulated with Dynabeads Human T-Activator CD3/CD28 and 10 ng/mL interleukin-2 were added. Tumorspheres and $CD8^+$ T cells were co-cultured for 96 h and changes in GFP intensity were acquired using a Nikon Eclipse Ti fluorescence microscope and measured using ImageJ software (Fiji (imagej.net)) Cell viability was determined using the Muse count and viability kit (Millipore). Alternatively, after incubation, tumor cells were harvested and stained using Annexin V/Propidium Iodide staining to assess the number of apoptotic or dead cells, determined by flow cytometry (BD LSR Fortessa Cell Analyzer).

Immunoblot analysis

Cells were lysed using RIPA buffer containing 1% protease inhibitor cocktail (Merck Millipore, MA) and 5% phosphatase inhibitor cocktail (Roche). Total protein concentration was measured using the Bradford protein assay (Quick Start Bradford Dye Reagent #5000205). The following antibodies were used: anti-IDO1, and anti-GAPDH (86630, and 51332, respectively, Cell Signaling Technology).

In vitro cell proliferation assays

For 3D spheroid proliferation assays, 500 cells/well were cultured in Corning Ultra-Low Attachment Surface 96 well plates (Corning Inc., Corning, NY) in 10μL of Neurobasal (Thermo Fisher Scientific) supplemented with Glutamine (Thermo Fisher Scientific), B27 (Thermo Fisher Scientific), 20 ng/mL epidermal growth factor (EGF) and fibroblast growth factor (FGF)-2 (PeproTech). After 24 h, 190μL of medium containing drug or vehicle were added. Tumor sphere growth was monitored and imaged every 24h using Nikon Eclipse Ti fluorescent microscope. The total area of tumor spheroids was analyzed using ImageJ software.

In vitro cell migration assays

For 3D spheroid cultures, 5,000 cells/well were cultured in Corning Ultra-Low Attachment Surface 96 well plates (Corning Inc., Corning, NY) in 100 μL of Neurobasal (Thermo Fisher Scientific) supplemented with Glutamine (Thermo Fisher Scientific), B27 (Thermo Fisher Scientific), 20 ng/mL epidermal growth factor (EGF) and fibroblast growth factor (FGF)-2 (PrepoTech). After 24 h, the medium was replaced with 50 μL of collagen I (Advanced BioMatrix, Inc San Diego, CA, USA) and neutralized to pH 7.5 using

1N NaOH and supplemented with FCS, penicillin-streptomycin, and 5 x DMEM. After polymerization, the collagen was overlaid with 50 μL of medium containing drug or vehicle. Migration of the cells outside the tumor spheroids were monitored and imaged every 24h using a Nikon Ti fluorescent microscope. For analysis and quantification ten images from each sample were selected and 10 areas measured from the rim of tumor to furthest point migrated using ImageJ software.

Quantitative real-time PCR analysis

Total RNA from mouse tumor tissues was extracted using TRIzol (Thermo Fisher Scientific). RNA was reverse-transcribed using iScript cDNA Synthesis Kit (BioRad) and quantitative real-time PCR was performed using SYBR Green Master Mix (Applied Biosystems). 18S expression levels were used as control. IDO1 expression was determined using following primers: mIDO1 Forward (CCAGTGCAGTAGAGCGTCAA); mIDO1 Reverse (TCTGGGTCCACAAAGTCACG).

In vivo studies

For survival studies, a total of 50,000 GL261fluc or CT2A cells were injected intracranially using a stereotactic frame in 3 μL Hanks' balanced salt solution (HBSS) 2 mm right lateral, 1 mm frontal to the bregma, and 3 mm deep in female C57/BL6 mice 7–8 or 28 weeks old. Fourteen days later, PPRX-1701 (10–20 mg/kg bodyweight) was injected intravenously three times per week, for a total of 2 weeks using insulin syringe with 8mm x 30G needle (BD Bioscience). Control cohort animals received treatment with the vehicle control nanoparticles. Successful tumor implantation was verified by bioluminescence imaging using the Perkin-Elmer IVIS Lumina and MRI. Each cohort consisted of 6 animals (total: 24 animals). Animals were distributed to the separate groups based on bioluminescence signal and body weight and treated in the same session and located in the same space in adjacent cages. The study endpoint was considered as a weight loss of 20%, onset of neurological symptoms, or signs of pain and distress.

MRI imaging

For the purpose of MRI, mice were anesthetized with isoflurane and MRI was performed using a BioSpec 3T MRI instrument (Bruker). The set-up 'mouse body RF coil with respiratory monitoring' was used. Images were acquired using the T2_TurboRARE sequence with the following settings: echo time: 47.73 ms, repetition time: 4993.715 ms, Rare Factor: 8, Averages: 3. Slice thickness: 0.5 mm, slicer orientation: axial. Field of View: 20 mm × 20 mm, Resolution: 0.078 mm × 0.078 mm. Images were extracted using the Horos open-source medical image viewer V.3.3.6, tumor volume was analyzed with the JiveX DICOM viewer (VISUS Health IT GmbH, Bochum, Germany).

Immunohistochemistry

Mice were euthanized using CO_2 inhalation and subsequently perfused with 4% neutral-buffered formalin (Sigma-Aldrich) for fixation. Cryoprotection was performed using 30% sucrose. All mouse brain slides were obtained from 30μm frozen sections. Slides were incubated with the primary antibody (1:50 in normal serum) overnight at 4°C. For detection of the primary antibody, species-matched fluorophore-coupled antibodies were incubated for 1 hour at room temperature. Slides were then covered with antifade mounting medium (Vectashield, Vector Laboratories) and cover slipped. All fluorescent and bright-field microscopy-based assays were observed using a Nikon Eclipse Ti microscope (Nikon). High-resolution confocal fluorescent microscopy was performed using a Zeiss LSM 710 confocal microscope system and visualized using ZEN Zeiss Imaging software.

Isolation of murine tumor-infiltrating leukocytes

The tumor-bearing right hemisphere was collected from each mouse on day 20 after tumor implantation. Each treatment cohort consisted of 4 animals (total: 16). A tumor dissociation kit for mouse (Miltenyi Biotec) was used for isolation of tumor infiltrating leukocytes according to the manufacturer's instructions. Harvested leukocytes were stored at −80°C until further use.

Mass cytometry (CyTOF)

All samples were thawed in a 37°C water bath and mixed with thawing media containing RPMI Medium 1640 (Life Technologies) supplemented with 5% heat-inactivated fetal bovine serum (Life Technologies), GlutaMAX (Life Technologies), antibiotic–antimycotic (Life Technologies), Minimum Essential Media (MEM) non-essential amino acids (Life Technologies), HEPES (4-(2-hydroxyethyl)-1-piperazineethanesulfonic acid) (Life Technologies), 2-mercaptoethanol (Sigma-Aldrich), sodium heparin (Sigma-Aldrich), and benzonase nuclease (Sigma-Aldrich). Aliquots of each sample post-thaw were mixed with PBS (Life Technologies) at a 1:1 ratio to be counted by flow cytometry. Between 0.5 and 2.0×10^6 cells were used for each sample. The samples were spun down and aspirated. Cisplatin viability staining reagent (Fluidigm) was added. Samples were fixed with 0.2% formaldehyde before staining. After centrifugation, mouse anti-CD16/32 antibody Fc-receptor blocking reagent (BioLegend) was used in cell staining buffer (CSB) (PBS with BSA (Sigma Aldrich) and sodium azide (Sigma Aldrich)) for 15 min followed by incubation with conjugated surface antibodies (each marker was used at a 1:100 dilution in CSB, unless stated otherwise) for 30 min. Samples were stained (see Table S1 for used markers), CD115, PD-1 and vascular endothelial growth factor receptor (VEGFR) were not detectable. All antibodies were obtained from the Harvard Medical Area CyTOF Antibody Resource and Core (Boston, Massachusetts, USA).

Samples were fixed with 4% formaldehyde before permeabilization with the FoxP3/Transcription Factor Staining Buffer Set (ThermoFisher Scientific) and were incubated with SCN (thiocyanate)–EDTA-coupled palladium-based barcoding reagents for

15 min and then combined into a single sample. Samples were incubated in a heparin solution for 15 min. Conjugated intracellular antibodies (each marker was used at a 1:100 dilution in permeabilization buffer, unless stated otherwise) were added into each tube and incubated for 60 min. Cells were then fixed with 4% formaldehyde for 10 min.

To identify single cell events, DNA was labeled for 20 min with an iridium intercalator solution (Fluidigm). Samples were subsequently washed and reconstituted in Maxpar Cell Acquisition Solution (Fluidigm) in the presence of EQ Four Element Calibration beads (Fluidigm) at a final concentration of 1×10^6 cells/mL. Samples were acquired on a Helios CyTOF Mass Cytometer (Fluidigm). Raw FCS files were normalized to reduce signal deviation over time, using the bead standard normalization method established by Fink et al.[48] The normalized files were then compensated with a panel-specific spillover matrix to subtract cross-contaminating signals, using the CyTOF-based compensation method.[49] These compensated files were then deconvoluted into individual sample files using a single-cell-based debarcoding algorithm.[50] Files were uploaded to OMIQ. In OMIQ, events were cleaned up using Gaussian parameters and then gated to remove normalization beads and to select live singlets. The latter were run through a principal component analysis for pre-embedding for an opt-SNE dimensionality reduction.26 From there, events were clustered using PARC27 to identify populations based on marker expression. Statistically different clusters between groups were identified using the multiclass setting of significance analysis of microarrays (SAM),[51] followed by statistical testing with Kruskal-Wallis rank-sum test with Dunn's multiple comparison; p values were adjusted with the Benjamini-Hochberg method. Differences in the separate leukocyte populations after treatment were assessed using a general linear model (GLM). For this, cell counts by group were exported and analyzed in the R package edgeR using the quasi-likelihood negative binomial generalized log-linear model. This was performed using the functions estimateDisp for dispersion estimation, glmQLFit to fit to the GLM, and glmQLFTest to run F-Tests on the fitted model.

Quantification of 6′-bromoindirubin-3′ acetoxime

Serum (20–50 μL) samples were prepared for 6′-bromoindirubin-3′ acetoxime quantification by adding 100–300 μL of acetonitrile. Tissue (60–350 mg) samples were extracted by adding 500–600 μL of acetonitrile and homogenizing with a tissue tearer. The samples were vortex mixed for 30 s, sonicated for 30 min, incubated at 4°C overnight, and then centrifuged for 5 min at 1,105 x g. The supernatant was transferred to an analysis vial. 6′-bromoindirubin-3′ acetoxime analysis was performed on a liquid chromatography Q-Exactive HFX Orbitrap mass spectrometer (LC-HRMS) (Thermo Scientific). Each extract was injected in triplicate 10 μL volumes. Sample components were separated on a C18 column (Thermo Hypersil Gold Vanquish, 50 mm × 2.1 mm x 1.9 μm) at a constant temperature of 60°C. Mobile phase A contained 2 mM aqueous ammonium acetate and mobile phase B contained 2 mM ammonium acetate in acetonitrile. 6′-bromoindirubin-3′ acetoxime eluted from the column at 4.77 min using a constant flow rate of 0.5 mL/min using a mobile phase gradient as follows: equilibration with 10% B until 1 min, increase to 55% B over 2 min and held for 0.3 min, increased to 100% over 1 min, and back to 10% B over 1.2 min and held for 1.5 min (total run time 6 min, data were collected from 0.05 to 6 min). The MS was operated in full scan dd-MS2 mode (30 NCE) with an inclusion list for 6′-bromoindirubin-3′ acetoxime, which included m/z 395.9989 as the quant ion and m/z 309.991 and 323.9909 as the confirming ions. Ionization was performed in negative mode with an ionization window of 4.0 m/z. Ions were further fragmented in the HCD collision cell filled with N2 (produced by a Peak Scientific Nitrogen Generator, Genius NM32LA). For the full-scan, the Orbitrap was operated with a resolution of 120,000. For dd-MS2, the Orbitrap was operated with a resolution of 15,000, AGC of 2x105, and maximum dwell time of 400ms. Quantification was performed in TraceFinder 5.0 General with external seven-point calibration curve prepared by serial dilutions of the calibration standard. The limit of detection (LOD) was determined from seven injections of a calibration standard and calculated as: LOD = [s * t (df, 1 – α = 0.99)]/m where s is the standard deviation, t is the student's t-value, df is the degrees freedom, α is the significance level (n = 7, α = 0.01, t = 3.14), and m is the slope of the calibration curve.[52] The extract LOD was 0.0563 μM.

Hematoxylin & eosin (H&E) staining of murine liver and spleen sections

Liver and spleen tissues were collected from C57/BL6 female mice implanted with GL261 cells and treated with either PPRX-1701 or control nanoparticles. At 24 h later, mice were euthanized, and spleen and liver tissues were collected and fixed in 10% formalin for 48 h and transferred to 30% sucrose for 24 h. Tissues were cryo-sectioned at 30μm of thickness and placed on slides. H&E staining was performed with the Hematoxylin & Eosin Stain Kit (H-3502, Vector Laboratories) by following the manufacturer's instructions. Sections were visualized at a magnification of 40× in a Nikon Eclipse Ti fluorescent microscope.

QUANTIFICATION AND STATISTICAL ANALYSIS

Graphs were generated and statistical analysis was performed using Prism (GraphPad). Statistical details of experiments, including number of experiments, statistical test and statistical significance (p value) are reported in the figure legends. Independent experiments were performed to define the reproducibility of the results.